EFFECT OF UNSHIELDED AND SHIELDED HORN BALANCES ON HINGE MOMENT COEFFICIENTS FOR CONTROLS AT LOW SPEEDS

1. NOTATION AND UNITS (see Sketch 1.1)

		SI	*British*
A_h	aspect ratio of horn, $s_h/\bar{c}_h$		
B	increase in balance due to horn (see Sketch 1.1)		
b_1	rate of change of hinge-moment coefficient with angle of attack	rad^{-1}	rad^{-1}
b_2	rate of change of hinge-moment coefficient with control deflection	rad^{-1}	rad^{-1}
Δb_{1h}	increment in b_1 due to horn balance	rad^{-1}	rad^{-1}
Δb_{2h}	increment in b_2 due to horn balance	rad^{-1}	rad^{-1}
$(b_1)_0{}^*/(b_1)_{0T}{}^*$	ratio of viscid to inviscid flow values of b_1 in two dimensions for aerofoil with $(t/c)_h = \tan \frac{1}{2}\tau_h$ (from Item No. Aero C.04.01.01)		
$(b_2)_0{}^*/(b_2)_{0T}{}^*$	ratio of viscid to inviscid flow values of b_2 in two dimensions for aerofoil with $(t/c)_h = \tan \frac{1}{2}\tau_h$ (from Item No. Aero C.04.01.02)		
C_H	hinge-moment coefficient, $H/\frac{1}{2}\rho V^2 S_f \bar{c}_f$		
$(c)_h$	wing chord at mid-span of horn	m	ft
$(c_b)_h$	chord of basic control (without horn) forward of hinge line at mid-span of horn (see Sketch 1.1)	m	ft
$\bar{c}_f$	mean chord of control aft of hinge line	m	ft
c_h	chord of horn forward of hinge line at mid-span of horn	m	ft
F_1, F_2	section thickness factors		
H	hinge moment, positive nose up	N m	lbf ft
N	nose shape correction factor		
K	correlating function depending on $(t/c)_h - \tan \frac{1}{2}\tau_h$		
R	Reynolds number based on wing mean chord		

Issued April 1988
With Amendments A to D, March 1997

S_f	area of control aft of hinge line	m^2	ft^2
s_f	span of control	m	ft
s_h	span of horn	m	ft
t	maximum section thickness	m	ft
$(t/c)_h$	thickness to chord ratio of wing at mid-span of horn		
V	free-stream velocity	m/s	ft/s
x_h	distance of horn leading edge ahead of trailing edge at mid-span of horn, as fraction of local wing chord		
ρ	density of air	kg/m^3	$slug/ft^3$
τ_h	trailing-edge angle at mid-span of horn	deg	deg

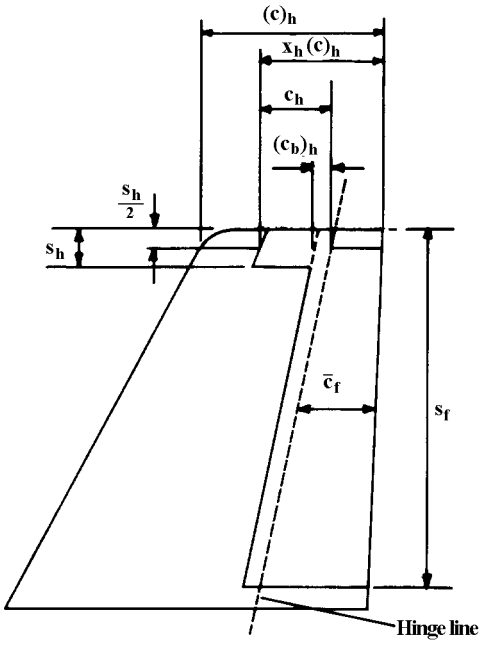

$$B = \left(\frac{s_h}{s_f}\right)\left(\frac{c_h}{\bar{c}_f}\right)^2\left[1-\left\{\frac{(c_b)_h}{c_h}\right\}^2\right]$$

Sketch 1.1

2. METHOD

This Item gives a semi-empirical method for predicting the increments in the rates of change of hinge-moment coefficient with angle of attack and control deflection, Δb_{1h} and Δb_{2h}, for horn balances fitted to the tips of unswept or moderately swept controls at low speeds. The increments are given in terms of the parameters $\Delta b_{1h}/A_h BF_1$ and $\Delta b_{2h}/A_h BF_2 NK$ which are presented in Figures 1 and 2, respectively, as functions of the horn leading-edge position x_h and span ratio s_h/s_f. The section thickness factors F_1 and F_2 are given in Figure 3 as functions of $(t/c)_h$. The function N is given in Figure 4 as a function of x_h and provides a correction for the different effects on Δb_{2h} of round-nosed and elliptically-nosed horns. The

function K is given in Figure 5 and allows for the effect of section shape on Δb_{2h} through the parameter $[(t/c)_h - \tan\tfrac{1}{2}\tau_h]$. The function K was determined primarily for application to unshielded horns, and for shielded horns the range of $[(t/c)_h - \tan\tfrac{1}{2}\tau_h]$ for which $K = 1$ should be taken to define a limit on applicability.

The method provides compatible predictions for the two types of horn, with the estimated values for the unshielded horns forming acceptable limiting values for shielded horns as x_h approaches unity. Because of the larger number of experimental data available, and its greater simplicity, a method restricted to unshielded horns was developed initially. A number of deductions from that analysis were then used in the construction of the method for shielded horns. This process is described in Section 2.1.

2.1 Development of Method

2.1.1 Unshielded horns

The method for unshielded horns has been developed by following Derivation 1 where the analysis of the hinge-moment data available when that report was published allowed $\Delta b_{1h}/A_h B$ and $\Delta b_{2h}/A_h B$ to be correlated linearly against $(t/c)_h$, the mean thickness to chord ratio of the wing over the span of the horn. Examination of information from Derivations 3, 5 and 6 that has become available since publication of Derivation 1 has now enabled different linear trends with $(t/c)_h$ to be established for Δb_{1h} and Δb_{2h}, but in the latter case with correction for trailing-edge angle. Thus Figures 1a and 2a give $\Delta b_{1h}/A_h B F_1$ and $\Delta b_{2h}/A_h B\ F_2 NK$ where the functions F_1 and F_2 are taken from Figure 3. These provide a better prediction for current control geometries. Almost all of the data studied were in the range $0.09 \le (t/c)_h \le 0.15$, but a linear extrapolation has been made to $(t/c)_h = 0.05$, where a single data point from Derivation 2 suggests that this is adequate.

In addition, empirical variations with the span ratio s_h/s_f, as shown in Figures 1a and 2a, have been determined to allow for the relatively larger effectiveness of horns with span ratio smaller than those considered in Derivation 2. These were established by looking at systematic tests in which a number of horns of different spans were tested with $(t/c)_h$ a constant.

The factor N is given in Figure 4 as a function of nose shape and is unity for unshielded horns, but is included in the ordinate of Figure 2a to give a consistent presentation with the data for shielded horns.

Most of the data examined were for section shapes for which $-0.01 \le [(t/c)_h - \tan\tfrac{1}{2}\tau_h] \le 0.04$. However, a set of tests reported in Derivation 5 on three pairs of models that were identical apart from large changes in control trailing-edge angle suggested that outside this range there was a pronounced variation in Δb_{2h}, but not in Δb_{1h}. The factor K in Figure 5 has been derived from those data, the part of the curve demonstrating the observed behaviour in Δb_{2h}. Because the shape of the curve has been deduced from a small number of data over a limited range of Reynolds number it must be taken as being indicative of trends rather than a precise correlation.

2.1.2 Shielded horns

The method for shielded horns has been developed similarly from the technique of Derivation 1. Again the parameters $\Delta b_{1h}/A_h B F_1$ and $\Delta b_{2h}/A_h B F_2 N$ are associated with F_1 and F_2, the same empirically determined functions of $(t/c)_h$, that were established for unshielded horns. The experimental data in Derivations 2 and 4 to 8 allow the parameters to be correlated in Figures 1b and 2b in terms of s_h/s_f and x_h. They show an increase in magnitude with decreasing s_h/s_f that is similar in form but somewhat faster than that for unshielded horns; their variation with x_h allows a smooth transition into the values for unshielded horns corresponding to $x_h = 1$. Regions of the carpets that have been interpolated by using the predictions for unshielded horns are shown dashed.

The factor N has been deduced from Derivation 2 which reports on a series of tests in which a number of otherwise identical horns were tested with elliptical or round (semi-circular) noses, for $s_h/s_f = 0.12$ and 0.24 and $0.5 \le x_h \le 0.85$. Those tests showed that the effect of nose shape on Δb_{2h} was significantly larger for the round-nosed horns. The higher curve for N shown in Figure 4 has been deduced to allow for this. In view of its limited data base it should only be regarded as tentative. The main body of data studied show that $N = 1$ is appropriate for horns with elliptical noses with minor to major axis ratios up to 0.3.

3. ACCURACY AND APPLICABILITY

3.1 Unshielded Horns

For unshielded horns Sketch 3.1 compares predicted and experimental values for the data used to construct the method and for many additional data contained in Derivation 1. The increments Δb_{1h} and Δb_{2h} are predicted to within about ± 0.05 rad^{-1} and ± 0.03 rad^{-1} respectively.

The rates of change of hinge-moment coefficient are defined for small angles of attack and control deflection, typically between $\pm 5°$. The ranges of geometric parameters examined in the preparation of the method are given in Table 3.1. All of the data were for full-span elevator and rudder controls with unswept hinge lines, but the method can be expected to apply equally well to ailerons and to controls with moderately swept hinge lines.

If the inboard edge of the horn is not parallel to the tip chord but inclined at a small angle ($\sim 10°$) so that the horn span varies between the control leading and the hinge line, then s_h should be taken as the mean span.

TABLE 3.1 Ranges of Experimental Data for Unshielded Horns

Parameter	*Range*	*Parameter*	*Range*
$(t/c)_h$	0.05 to 0.15	A_h	0.32 to 1.20
τ_h	5° to 20°	B	0.04 to 0.35
$[(t/c)_h - \tan \tfrac{1}{2}\tau_h]$	–0.32 to 0.074	R	10^6 to 4×10^6
s_h/s_f	0.07 to 0.25		

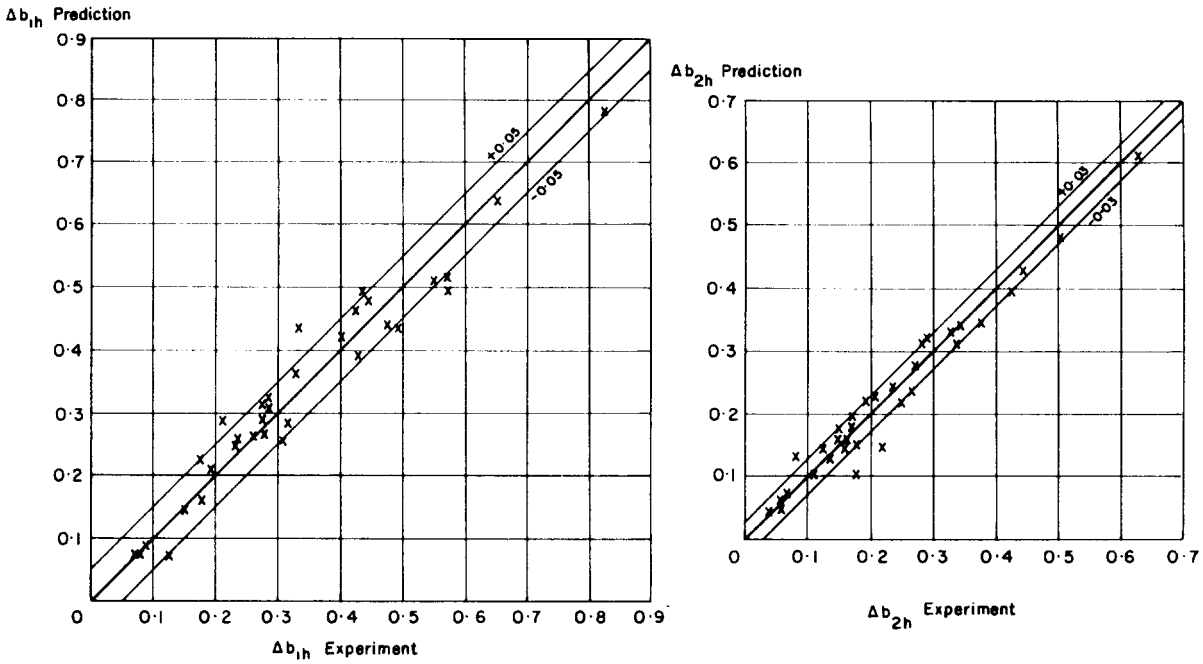

Sketch 3.1 Comparison of predicted and experimental values for unshielded horns

3.2 Shielded Horns

For shielded horns Sketch 3.2 compares predicted and experimental values for the data used to develop the method. In general both increments are predicted to within about ± 0.025 rad^{-1}, although the overall scatter is slightly greater for Δb_{2h}, most notably for round-nosed horns. This emphasises that the factor N must be used with caution, especially for horns of small span ratio, $s_h/s_f < 0.12$, because as explained in Section 2.1.1 it has been derived from a single limited set of test data. The greater scatter for Δb_{2h} is also partly due to the fact that the variation of Δb_{2h} with horn geometry is less consistent than that of Δb_{1h}. Where there is conflict in the data the shape of Figure 1b has been used as a guide in the construction of Figure 2b.

A number of experimental data, shown as circles in Sketch 3.2, have values of Δb_{1h} and Δb_{2h} that are much lower than predicted. No fully satisfactory explanation has been found for this but those tests were for low Reynolds number ($\leq 0.6 \times 10^6$) and for section geometries such that the ratio of the two-dimensional viscid to inviscid hinge moment coefficient derivatives, $(b_1)_0{}^*/(b_1)_{0T}{}^*$ and $(b_2)_0{}^*/(b_2)_{0T}{}^*$, as estimated from Item Nos Aero C.04.01.01 and 02 (Derivations 9 and 10), were as low as 0.16 and 0.26 respectively. The main body of the data for shielded horns (and all of the data for unshielded horns), satisfied the conditions $(b_1)_0{}^*/(b_1)_{0T}{}^* > 0.35$ and $(b_2)_0{}^*/(b_2)_{0T}{}^* > 0.45$. It is therefore suggested that the method should only be used when those conditions are met.

For all of the test data that have been studied on shielded horns it was satisfactory to assume that $K = 1$. However, it was found during the study of unshielded horns that, if a configuration failed to satisfy the criterion $-0.01 \leq [(t/c)_h - \tan \tfrac{1}{2}\tau_h] \leq 0.04$, the adjustment to K in Figure 5 was required for a successful prediction of Δb_{2h}. In the absence of test data to investigate this matter for shielded horns it is recommended that the above range be taken as a limit on applicability.

The rates of change of hinge-moment coefficient are defined for small angles of attack and control deflection, typically between $\pm 5°$. The limited data that have been studied indicate, however, that the variation of the hinge-moment coefficient is essentially linear for angles of attack up to about 10° in magnitude and for control deflections up to about 8° in magnitude. The actual limits will depend on individual control geometry, particularly in respect of control deflection, as some non-linearity can be expected to occur as the horn unports.

The ranges of parameters examined in the preparation of the Item are given in Table 3.2. All the data were for controls with unswept or moderately swept hinge lines ($\leq 30°$). The horn planforms were all similar to that shown in Sketch 1.1, the inboard and outboard edges of the horn being parallel to the root chord of the main surface and its leading edge lying along a constant percentage chord line.

TABLE 3.2 Ranges of Experimental Data for Shielded Horns

Parameter	*Range*	*Parameter*	*Range*
$(t/c)_h$	0.05 to 0.15	A_h	0.6 to 3.6
τ_h	6° to 16°	B	0.008 to 0.20
$[(t/c)_h - \tan \frac{1}{2}\tau_h]$	–0.006 to 0.025	R	0.6×10^6 to 2.3×10^6
s_h/s_f	0.07 to 0.24	x_h	0.48 to 0.86

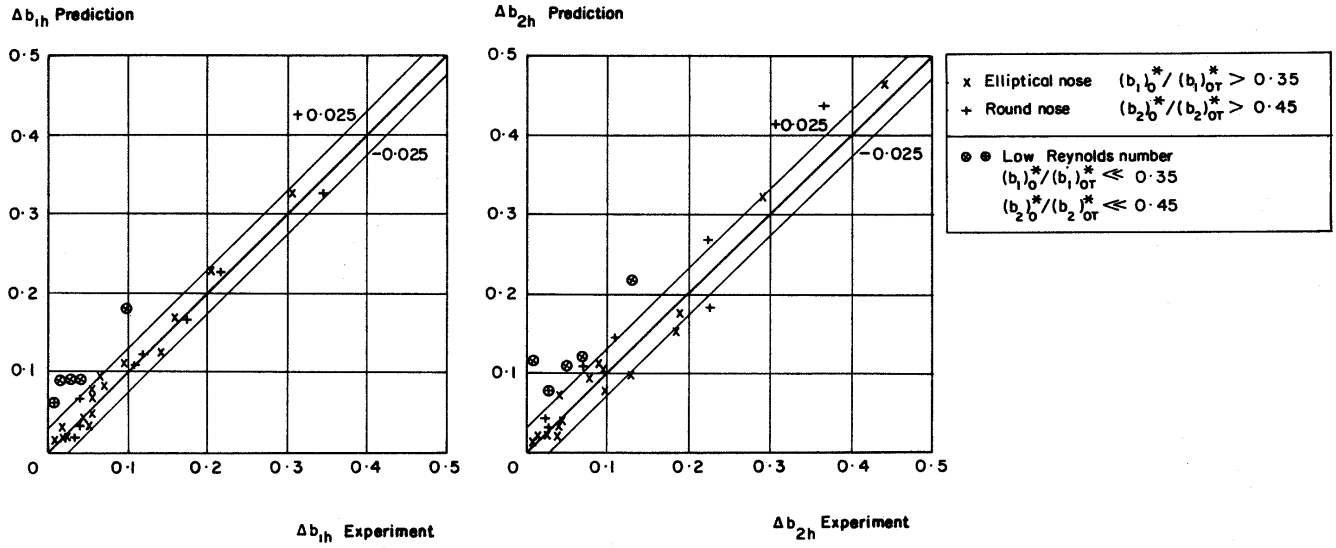

Sketch 3.2 Comparison of predicted and experimental values for shielded horns

4. DERIVATION

The Derivation lists selected sources that have assisted in the preparation of this Item.

1. THOMAS, H.H.B.M. LOFTS, M. — Analysis of wind tunnel data on horn balance. RAE Rep. Aero. 1994, (ARC 8422), 1944.

2. LOWRY, J.G. MALONEY, J.A. GARNER, I.E. — Wind-tunnel investigation of shielded horn balances and tabs on a 0.7 scale model of the XF6F vertical tail surface. NACA ACR 4C11, 1944.

3. LOWRY, J.G. CRANDALL, S.M. — Wind tunnel investigation of unshielded horn balances on a horizontal tail surface. NACA tech. Note 1377, 1947.

4. CLEARY, J.W.
KRUMM, W.J.
High speed aerodynamic characteristics of horn and overhang balances on a full-scale elevator. NACA RM A7H29 (TIL 1563), 1948.

5. HARPER, J.J.
Wind-tunnel investigation of effects of various aerodynamic balance shapes and sweepback on control surface characteristics of semi span tail surfaces with NACA 0009, 0015, 66–009 66(215)–014, and circular arc airfoil sections. NACA tech. Note 2495, 1949.

6. BAe
Unpublished wind-tunnel data.

7. SHORT BROTHERS
Unpublished wind-tunnel data.

8. SAAB-SCANIA
Unpublished wind-tunnel data.

ESDU Items

9. ESDU
Rate of change of hinge-moment coefficient with incidence for a plain control in incompressible two-dimensional flow, $(b_1)_0$. Item No. Aero C.04.01.01. ESDU International, London, 1956.

10. ESDU
Rate of change of hinge-moment coefficient with control deflection for a plain control in incompressible two-dimensional flow, $(b_2)_0$. Item No. Aero C.04.01.02. ESDU International London, 1956.

5. EXAMPLES

5.1 Example I

Calculate the effect on the rates of change of hinge-moment coefficient due to the unshielded horn balance fitted to the rudder shown in Sketch 5.1.

It can be assumed that at the horn mid-span the fin has section properties $(t/c)_h = 0.10$ and $\tau_h = 11.0°$.

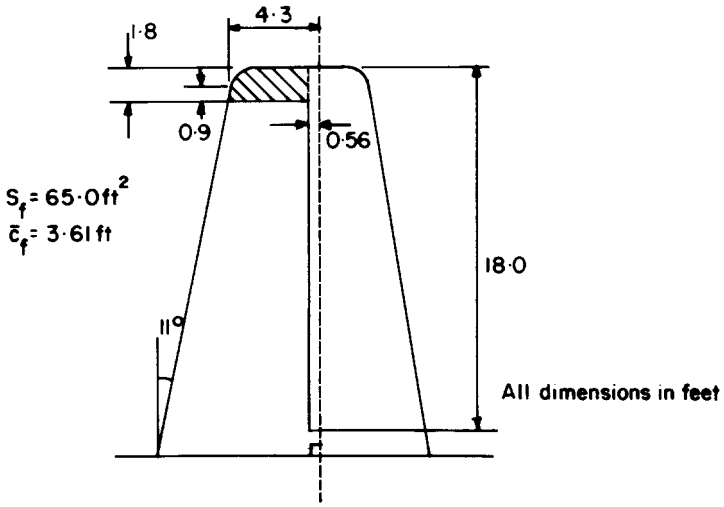

Sketch 5.1 Fin and rudder geometry

From Sketch 5.1 the mean chord of the horn is $\bar{c}_h = 4.3\text{ft}$.

The aspect ratio of the horn is

$$A_h = s_h/\bar{c}_h = 1.8/4.3 = 0.419,$$

and it causes an increase in balance

$$B = \left(\frac{s_h}{s_f}\right)\left(\frac{c_h}{\bar{c}_f}\right)^2\left[1-\left\{\frac{(c_b)_h}{c_h}\right\}^2\right]$$

$$= \left(\frac{1.8}{18.0}\right)\left(\frac{4.3}{3.61}\right)^2\left[1-\left\{\frac{0.56}{4.3}\right\}^2\right] = 0.139.$$

From Figure 1a, for $s_h/s_f = 1.8/18.0 = 0.1$,

$$\Delta b_{1h}/A_h BF_1 = 1.45,$$

and from Figure 2b

$$\Delta b_{2h}/A_h BF_2 NK = 1.08.$$

From Figure 3, for $(t/c)_h = 0.10$,

$$F_1 = 3.74 \text{ and } F_2 = 2.86.$$

For an unshielded horn $N = 1$, and as $[(t/c)_h - \tan\tfrac{1}{2}\tau_h] = 0.10 - 0.096 = 0.004$ lies between – 0.01 and 0.04, Figure 5 gives $K = 1$.

Therefore

$$\Delta b_{1h} = 1.45 \times 0.419 \times 0.139 \times 3.74 = 0.315 \text{ rad}^{-1},$$

and

$$\Delta b_{2h} = 1.08 \times 0.419 \times 0.139 \times 2.86 \times 1.0 \times 1.0 = 0.180 \text{ rad}^{-1}$$

5.2 Example II

Calculate the effect on the rates of change of hinge-moment coefficient with incidence and control deflection due to the shielded horn balance fitted the rudder shown in Sketch 5.2. It can be assumed that the horn has an elliptical nose and the fin has mean section properties $(t/c)_h = 0.10$ and $\tau_h = 11.0°$ at the mid-span of the horn. Examine the effect of rounding the horn nose.

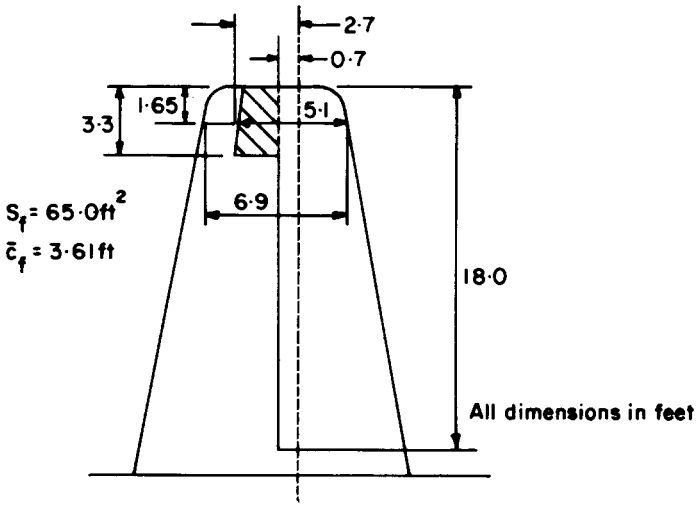

Sketch 5.2 Fin and rudder geometry

A preliminary check on applicability (see Section 3.2) confirms that $[(t/c)_h - \tan \tfrac{1}{2}\tau_h] = 0.10 - 0.096 = 0.004$ lies satisfactorily between –0.01 and 0.04.

From Sketch 5.2 the aspect ratio of the horn is

$$A_h = s_h/\bar{c}_h = 3.3/2.7 = 1.22\,.$$

It causes an increase in balance

$$B = \left(\frac{s_h}{s_f}\right)\left(\frac{c_h}{\bar{c}_f}\right)^2\left[1-\left\{\frac{(c_b)_h}{c_h}\right\}^2\right]$$

$$= \left(\frac{3.3}{18.0}\right)\left(\frac{2.7}{3.61}\right)^2\left[1-\left\{\frac{0.7}{2.7}\right\}^2\right] = 0.096\,,$$

has a leading-edge position

$$x_h = 5.1/6.9 = 0.74,$$

and a span ratio

$$s_h/s_f = 3.3/18.0 = 0.183.$$

Using the last two results, Figures 1b and 2b give, respectively,

$$\frac{\Delta b_{1h}}{A_h B F_1} = 0.285 \text{ rad}^{-1}$$

and

$$\frac{\Delta b_{2h}}{A_h B F_2 N K} = 0.455 \text{rad}^{-1}\,.$$

With $(t/c)_h = 0.10$, Figure 3 gives $F_1 = 3.74$ and $F_2 = 2.86$,

and, since the horn has an elliptical nose, $N = 1.0$.

As $-0.01 \leq [(t/c)_h - \tan \tfrac{1}{2}\tau_h] \leq 0.04$, $K = 1$.

Therefore

$$\begin{aligned} \Delta b_{1h} &= 0.285 \times 1.22 \times 0.096 \times 3.74 \\ &= 0.125 \text{ rad}^{-1}, \end{aligned}$$

and

$$\begin{aligned} \Delta b_{2h} &= 0.455 \times 1.22 \times 0.096 \times 2.86 \times 1.0 \times 1.0 \\ &= 0.152 \text{ rad}^{-1}. \end{aligned}$$

for a round-nosed horn with $x_h = 0.74$, Figure 4 gives $N = 1.49$.

In that case $$\begin{aligned} \Delta b_{2h} &= 0.455 \times 1.22 \times 0.098 \times 2.86 \times 1.49 \times 1.0 \\ &= 0.227 \text{ rad}^{-1}, \end{aligned}$$

an increase of 0.075 rad^{-1} in the increment due to the horn.

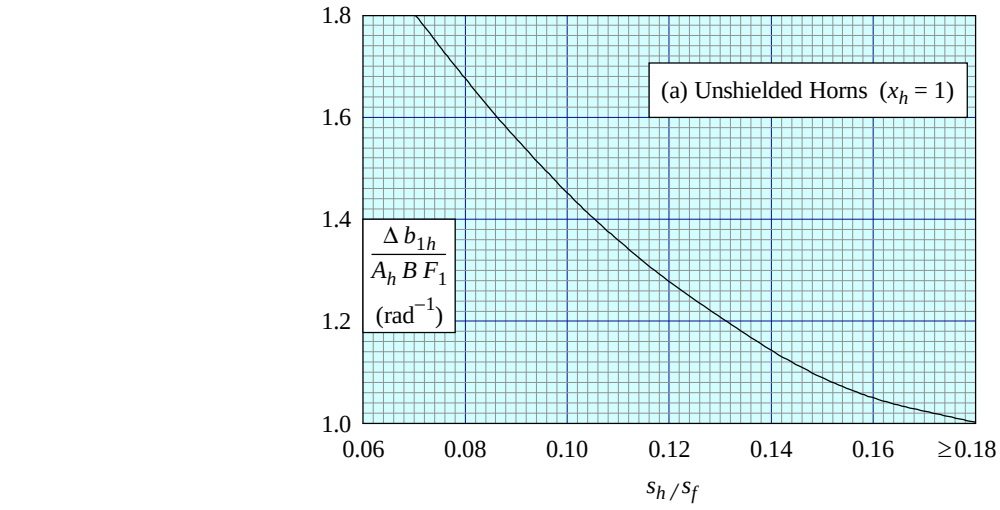

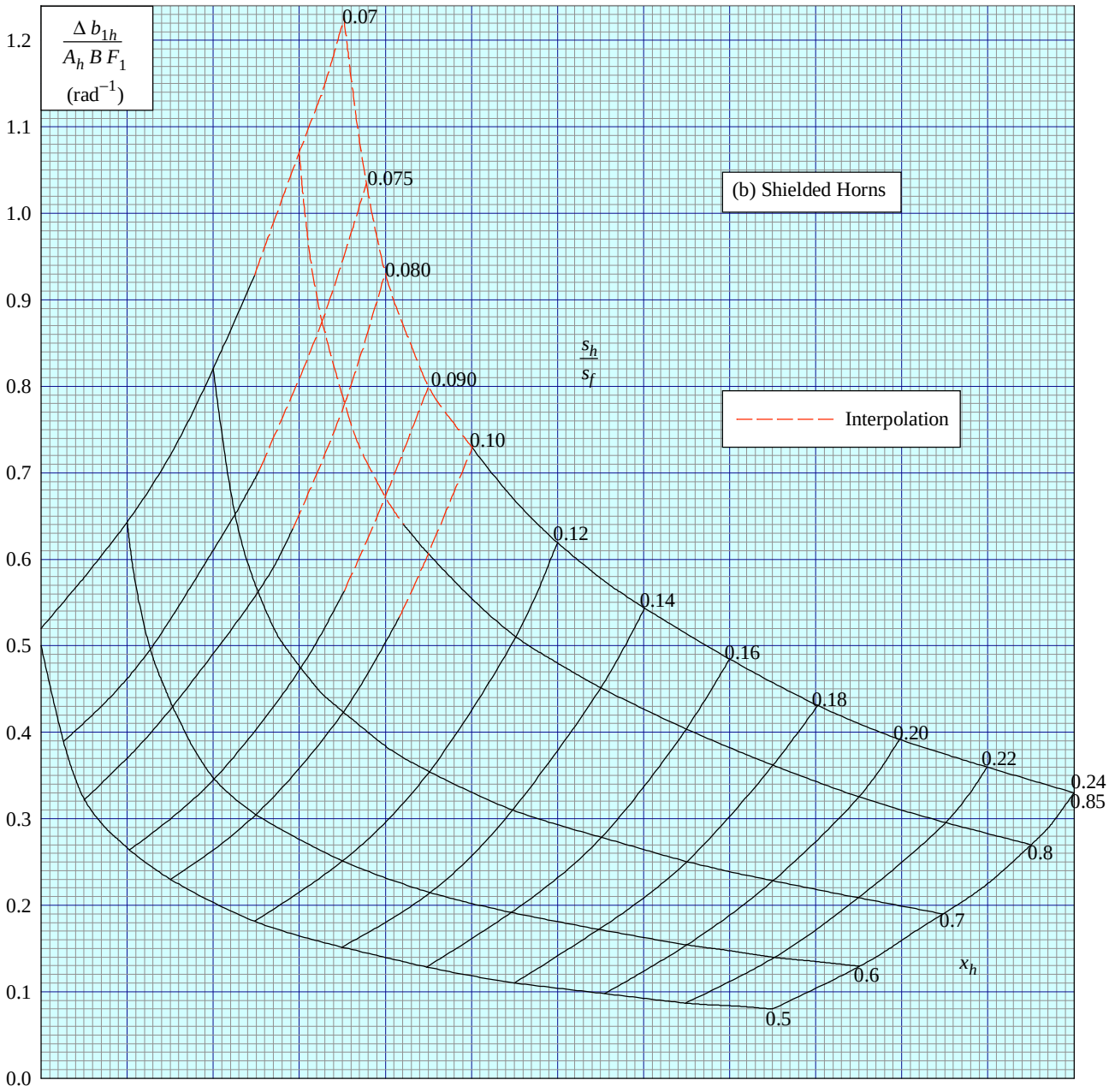

FIGURE 1 HINGE MOMENT COEFFICIENT DERIVATIVE DUE TO ANGLE OF ATTACK

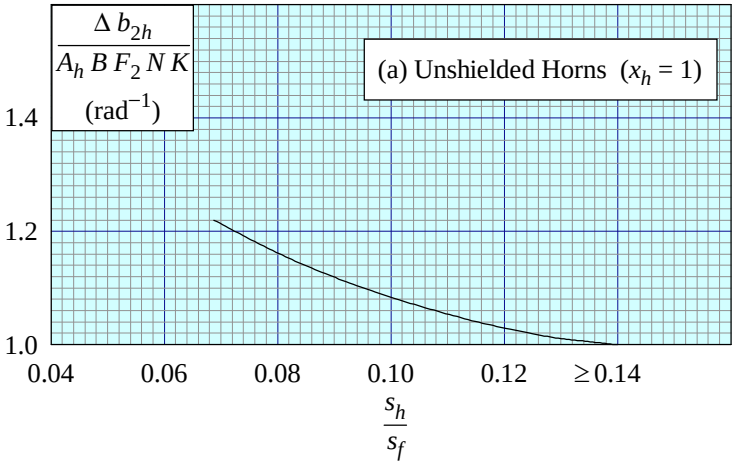

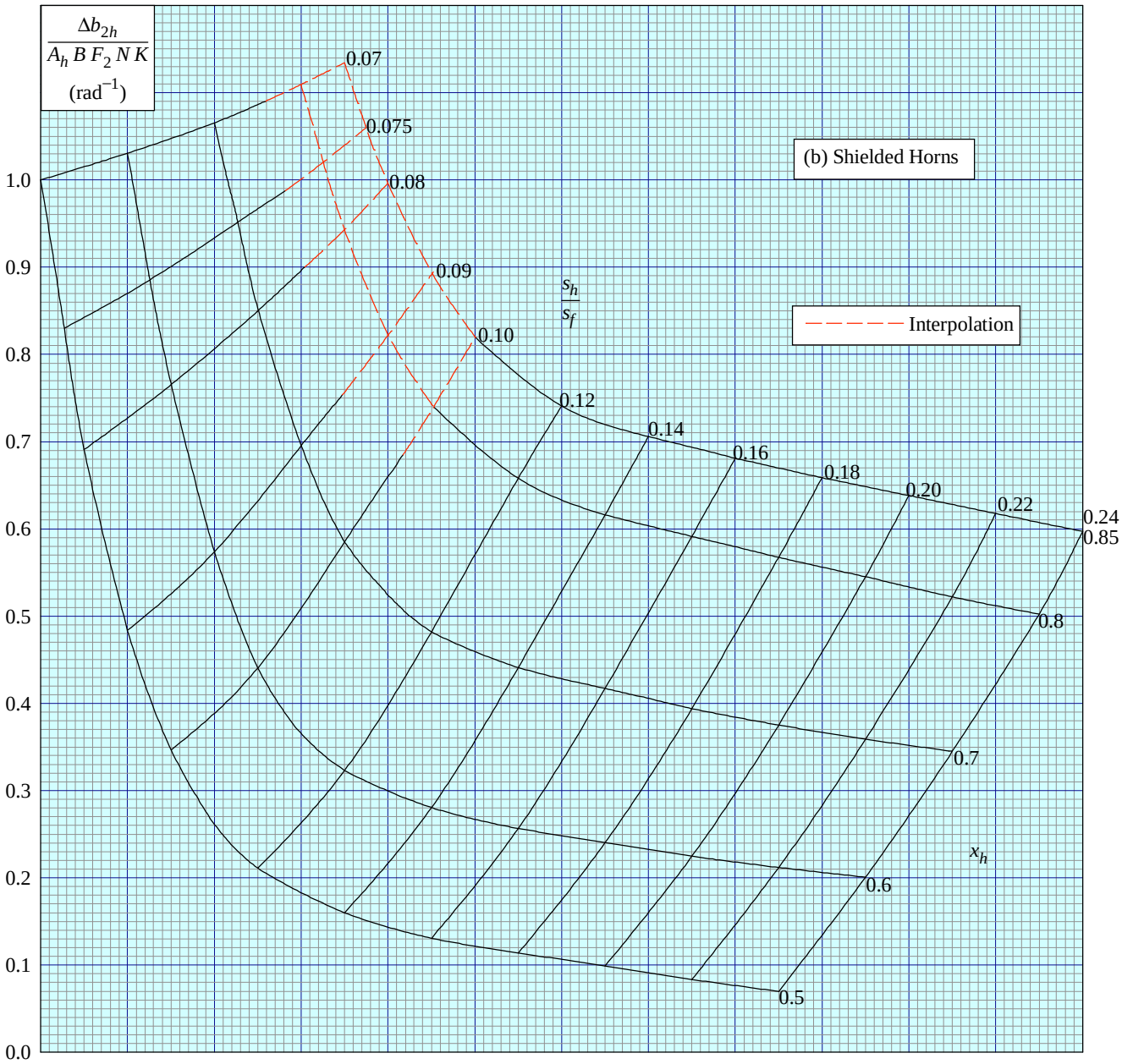

FIGURE 2 HINGE MOMENT COEFFICIENT DERIVATIVE DUE TO CONTROL DEFLECTION

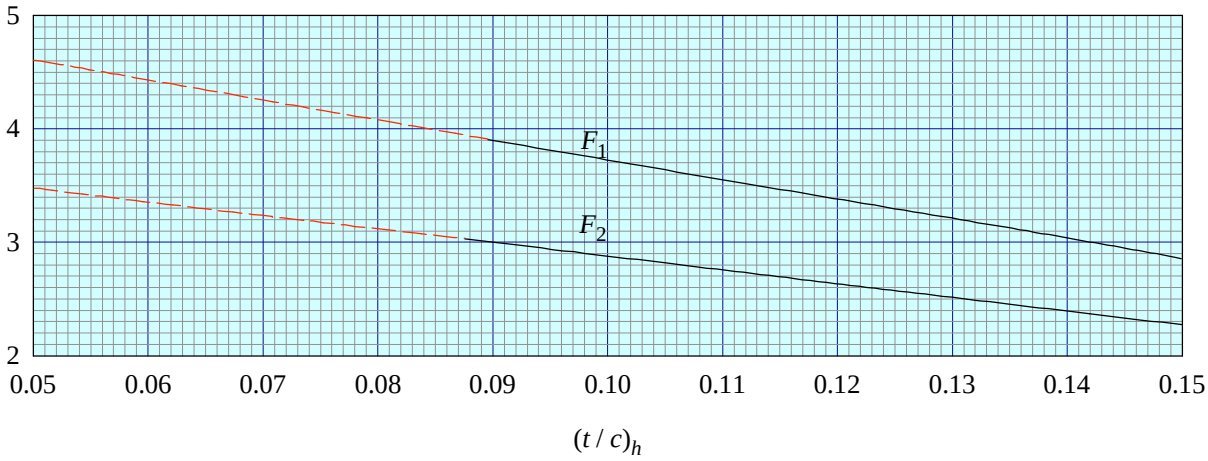

FIGURE 3 SECTION THICKNESS FACTORS

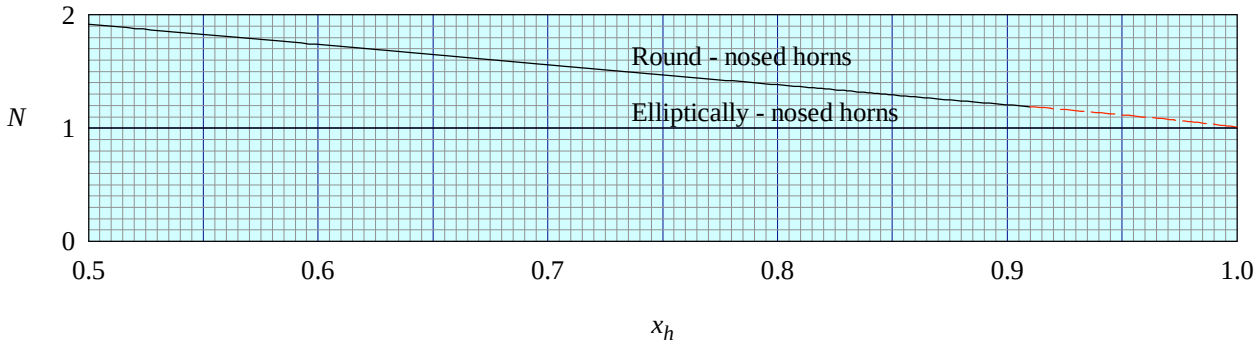

FIGURE 4 NOSE SHAPE CORRECTION FACTOR

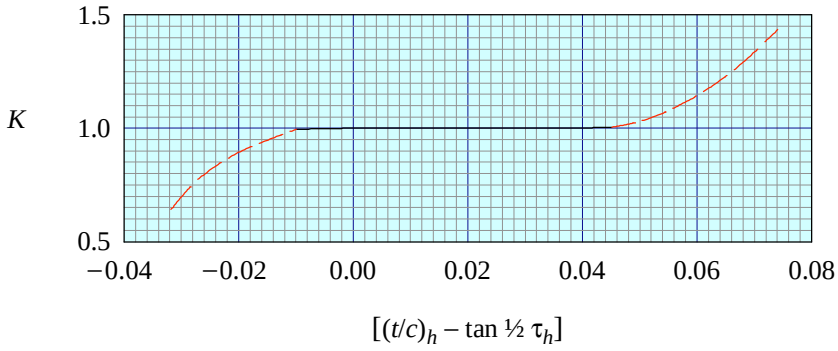

FIGURE 5 SECTION SHAPE CORRECTION FACTOR

THE PREPARATION OF THIS DATA ITEM

The work on this particular Item, which supersedes Item No. 87032 and Item No. Aero C.04.01.07, was monitored and guided by the Aerodynamics Committee which first met in 1942 and now has the following membership:

Chairman

Mr H.C. Garner	–	Independent

Vice-Chairman

Mr P.K. Jones	–	British Aerospace plc, Civil Aircraft Div., Woodford

Members

Mr G.E. Bean*	–	Boeing Aerospace Company, Seattle, Wash., USA
Mr E.A. Boyd	–	Cranfield Institute of Technology
Mr K. Burgin	–	Southampton University
Mr W.S. Chen*	–	Northrop Corporation, Hawthorne, Calif., USA
Dr T.J. Cummings	–	Short Brothers plc
Mr J.R.J. Dovey	–	Independent
Mr L. Elmeland*	–	Saab-Scania, Linköping, Sweden
Dr J.W. Flower	–	Bristol University
Mr P.G.C. Herring	–	Sowerby Research Centre, Bristol
Mr R. Jordan	–	Aircraft Research Association
Mr J.R.C. Pedersen	–	Independent
Mr N. Roberts	–	Rolls-Royce plc, Derby
Mr R. Sanderson	–	Messerschmitt-Bölkow-Blohm GmbH, Hamburg, W. Germany
Mr A.E. Sewell*	–	McDonnell Douglas, Long Beach, Calif., USA
Mr M.R. Smith	–	British Aerospace plc, Military Aircraft Div., Weybridge
Miss J. Willaume	–	Aérospatiale, Toulouse, France.

* Corresponding Member

The technical work involved in the assessment of the available information and the construction and subsequent development of the Data Item was undertaken by

Mr R.W. Gilbey	–	Senior Engineer.